iScience

CellPress
OPEN ACCESS

Article

Opportunity of rooftop solar photovoltaic as a cost-effective and environment-friendly power source in megacities

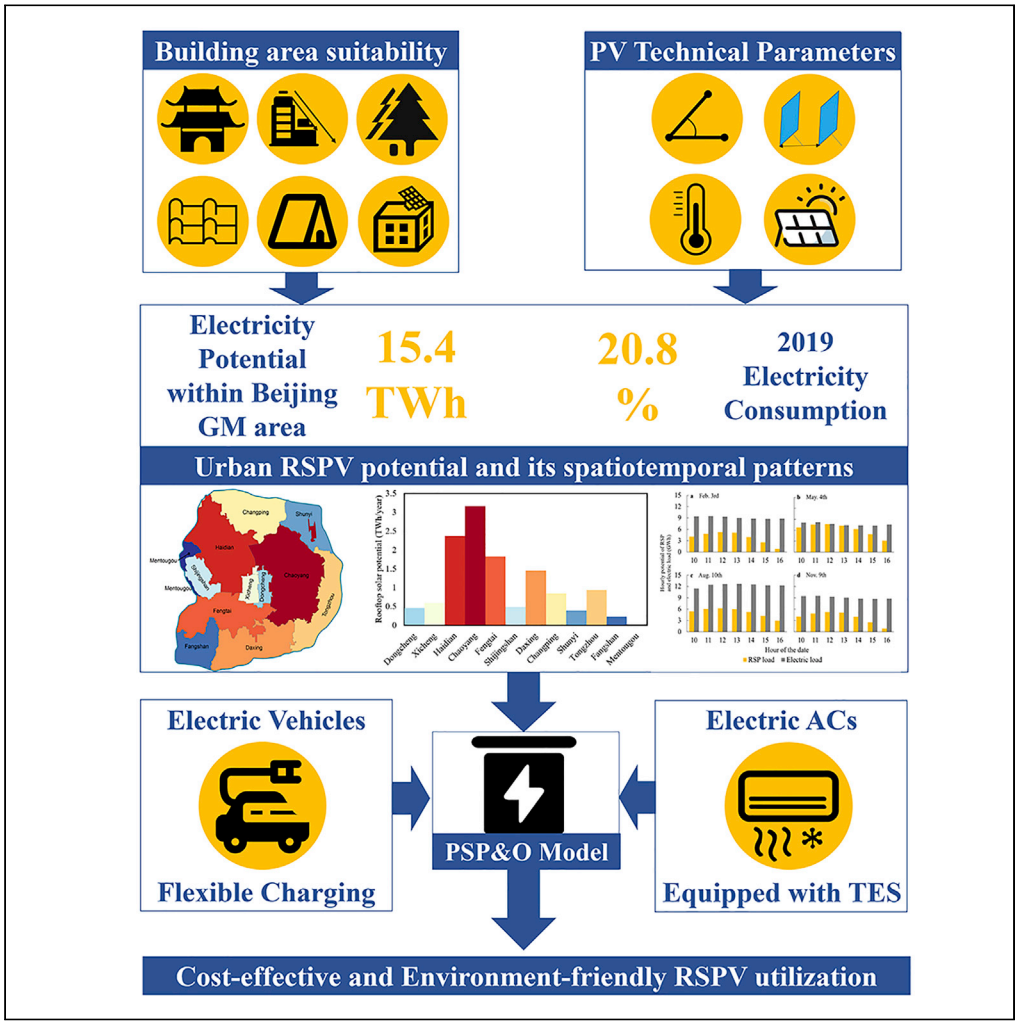

Mai Shi, Xi Lu, Haiyang Jiang, ..., Ning Zhang, Ye Wu, Aoife M. Foley

xilu@tsinghua.edu.cn (X.L.)
ningzhang@tsinghua.edu.cn (N.Z.)
a.foley@qub.ac.uk (A.M.F.)

Highlights

Develop a building-level RSPV potential assessment model for mega-cities

Show the chance to fully use RSPV potential cost-effectively and environment-friendly

The RSPV potential in the Beijing GM area amounts to 20.8% of the power demand

Deployment of RSPV + system would reduce the required new transmission capacity

Shi et al., iScience 25, 104890
September 16, 2022 © 2022
https://doi.org/10.1016/j.isci.2022.104890

iScience

CellPress
OPEN ACCESS

Article

Opportunity of rooftop solar photovoltaic as a cost-effective and environment-friendly power source in megacities

Mai Shi,[1,2,3] Xi Lu,[1,2,3,7,*] Haiyang Jiang,[4] Qing Mu,[1,2,3] Shi Chen,[1,2,3] Rachael Marie Fleming,[1] Ning Zhang,[4,*] Ye Wu,[1] and Aoife M. Foley[5,6,*]

SUMMARY

Rooftop solar photovoltaics (RSPV) are critical for megacities to achieve low-carbon emissions. However, a knowledge gap exists in a supply-demand-coupled analysis that considered simultaneously RSPV spatiotemporal patterns and city-accommodation capacities, a pivotal way to address solar PV intermittency issues. Here, we developed an aggregated model for an RSPV + system by linking building-level potential assessment to dynamic optimization of building-related flexible loads. Taking Beijing, the capital city of China, as case in point, we show that annual RSPV potential in Beijing's Greater-Metropolitan area amounts to 15.4 TWh, all of which could be accommodated environmentally friendly and cost-effectively through the smart operation of electric vehicles and air conditioners equipped with thermal energy storage (TES). Additionally, the RSPV + system would reduce the 8.6 GW transmission capacity otherwise required for increasing electricity demand for 2035 in Beijing. The analysis offers an important reference for sustainable RSPV development in mega-cities in China and other countries globally.

INTRODUCTION

As the world's largest CO_2 emitting country, China accounts for about 28.8% of global carbon emissions (British Petroleum, 2020). Decarbonization of China's economy is pivotal in realizing the climate goals to limit the global average surface temperature rise well below 2 °C or within 1.5 °C by the end of this century. In 2020, China announced the target to realize carbon neutrality by 2060, which demands short-term development of no less than 1.2 TW of renewable (wind and solar) capacity to be installed by 2030, and greater expansion of renewable energy sources in the longer term (World Resource Institute, 2020). As the largest PV panel manufacturer in the world, China also plans to reach a total of 5000 GW PV capacity in 2050 (Wang, 2019). As a locally available and renewable power resource for urban residents, rooftop solar photovoltaics (RSPV) are receiving attention from decision-makers and the public in Chinese cities, where approximately 85% of the country's energy is consumed (China Urban Energy Report Research Group, 2019). The installed capacity of distributed PV (mainly RSPV) in China has increased from 4.7 GW in 2014 to 79.9 GW in 2020, the latter of which accounted for 32.5 and 11.3%, respectively, of the cumulative PV capacity in China and globally (National Energy Administration, 2021; International renewable energy agency, 2021). Many mega-cities in China, including Beijing, have given high priority to the deployment of RSPV to fulfill their carbon peaking and carbon neutrality targets (The People's Government of Beijing Municipality, 2020).

However, large-scale integration of RSPV may pose challenges to existing power grids owing to its inherent intermittency (Obi and Bass, 2016). A duck curve phenomenon happened in the power grid of California Independent System Operator with the relatively high penetration of RSPV, which is featured by steep power ramps and shortened capacity for the frequency response (Folsom, 2013). A number of case studies in Britain, US, Spain, and Australia further indicated that high penetration of RSPV, if not properly handled, would distort electricity market prices and incur significant financial loss (Sharma et al., 2020; Dimitriadis, 2015; Unión Española Fotovoltaica., 2018; Joskow., 2018). Therefore, future RSPV development requires the urban RSPV evaluation to be more practical, from simply answering the total potential to precisely quantifying its spatiotemporal distribution and its effective utilization. Effective utilization of RSPV requires

[1]School of Environment, State Key Joint Laboratory of Environment Simulation and Pollution Control, Tsinghua University, Beijing 100084, China

[2]Institute for Carbon Neutrality, Tsinghua University, Beijing 10084, P.R. China

[3]Beijing Laboratory of Environmental Frontier Technologies, Tsinghua University, Beijing 100084, China

[4]State Key Lab of Power Systems, Department of Electrical Engineering, Tsinghua University, Beijing 100084, China

[5]School of Mechanical and Aerospace Engineering, Queen's University, Belfast, Northern Ireland BT9 5AH, UK

[6]Department of Civil, Structural, and Environmental Engineering, Trinity College Dublin, The University of Dublin, Ireland

[7]Lead contact

*Correspondence: xilu@tsinghua.edu.cn (X.L.), ningzhang@tsinghua.edu.cn (N.Z.), a.foley@qub.ac.uk (A.M.F.)

https://doi.org/10.1016/j.isci.2022.104890

coordinated consideration of both the high-resolution spatiotemporal features of the RSPV potential and the accommodation capacity from the electrical loads. The evaluation framework with high spatiotemporal resolution can not only provide important guidance for RSPV development and planning on a city scale but also detailed location information for the potential future expansion of distribution facilities of the electric grid power system. In addition, the estimated hourly RSPV outputs could support the optimization of RSPV dynamic utilization with hourly electrical loads.

Although existing studies have investigated the urban RSPV application, a potential-utilization integrated analysis remains a literature gap. Existing studies tended to treat supply and consumption separately, with a focus on either assessment of RSPV resources, or quantification of potential urban accommodation capacity. In general, the studies on urban RSPV potential assessment fell into three categories: (1) hybrid framework with sampling method that examined features from individual building samples of small city blocks and then applied to the entire urban area or even national and global scale based on population, roadmap and building density, (2) building typology assignment that classified buildings into different types and assigned corresponding availability factors to each type of rooftop, and (3) GIS-based that either characterized the structure and shade of rooftop areas based on high-resolution LIDAR data and digital surface model data to directly evaluate the potential for RSPV, or captured rooftop geometry through artificial analysis of remote sensing data (Gagnon et al., 2016; Defaix et al., 2012; Wiginton et al., 2010; Ghosh et al., 2006; Vardimon, 2011; Li et al., 2015; Song et al., 2018; Ordóñez et al., 2010; Kouhestani et al., 2019; Lee et al., 2018; Byrne et al., 2015; Bergamasco and Asinari, 2011; Peng and Lu, 2013; Izquierdo et al., 2008; Guo., 2015; Denholm et al., 2009; Singh and Banerjee, 2015; Zhang, 2017; Levinson et al., 2009; Fogl Moudrý, 2016; Joshi et al., 2021; Bódis et al., 2019; Mohajeri et al., 2018; Zhong et al., 2021). For mega-cities in China, knowledge gaps still exist for RSPV potential evaluation with high spatiotemporal resolution, which considers the building-scale suitability spatially and provides the RSPV power outputs over 8760 h for a full year. In addition, studies addressed the opportunities from smartly operating electrical loads, such as electric vehicles (EVs), air conditioners (ACs), and other flexible loads to effectively use the variable power from RSPV (Litjens et al., 2018; Good et al., 2019; Shepero et al., 2020; Laine et al., 2019; Martin et al., 2022). However, they focus on individual buildings or communities and fail in characterizing the RSPV spatiotemporal features at the city level, and rarely conduct optimization models fully considering the 8760-h optimization on daily and seasonal variation of power generation and loads.

In this study, we developed a potential-utilization linked framework to investigate the opportunity for RSPV in mega-cities, by linking a high spatiotemporal resolution RSPV potential assessment module with a dynamic utilization optimization module (see Figure 1). A suite of impact factors for individual buildings were considered on hourly basis, such as building and tree shadows, roof structure and slope, and so forth. Building on this, we further applied the power system planning & optimization (PSP&O) model to investigate the synergy between the RSPV power and emerging urban loads from EVs and ACs by considering the latter's dynamic compensation effects on the former. Here, we took Beijing, the capital city of China, as case in point, and demonstrated a win-win situation that the locally available RSPV with a potential of 15.4 TWh in the Greater Metropolitan area (GM) of Beijing could be effectively utilized by the growing electricity demand from EVs and ACs equipped with thermal energy storage (TES) in the city in 2035, the target year of China's Long-range Objectives for national economic and social development (2021-2035). Here, the GM area refers to the area inside 6th Ring Road (RD6) in Beijing, which mainly consists of the densely populated city area (inside RD5) and so-called "in-between city" area (Sieverts, 2003) (RD6-RD5). In Beijing, approximately 70% of electricity consumption relies on external power primarily generated from the coal-fired power plants in the northern electric power grid in China (The People's Government of Beijing Municipality, 2013). Should all the RSPV potential be utilized in Beijing to substitute the external coal-fired power, emissions of 16.4 Mt CO_2, 6.2 kt NO, 2.9 kt SO_2, and 1.3 kt $PM_{2.5}$ would be reduced annually, and at the same time, 8.6 GW capacity for transmission lines to Beijing can be avoided for construction. An extended statistical analysis of urban RSPV for 344 cities at the prefecture level in the Chinese mainland indicates a total potential of 531TWh, corresponding to 7.3% of the total electricity demand in these cities.

RESULT

Potential for rooftop solar photovoltaics power

Beijing GM area (inside RD6), which accounts for 80.2% of population and 13.8% of the jurisdiction area of the entire city (Beijing Municipal Bureau of Statistics, 2018), has approximately 125 km^2 of the total of 235 km^2 rooftop areas identified suitable for the deployment of RSPV. As illustrated in Figure 2D, the

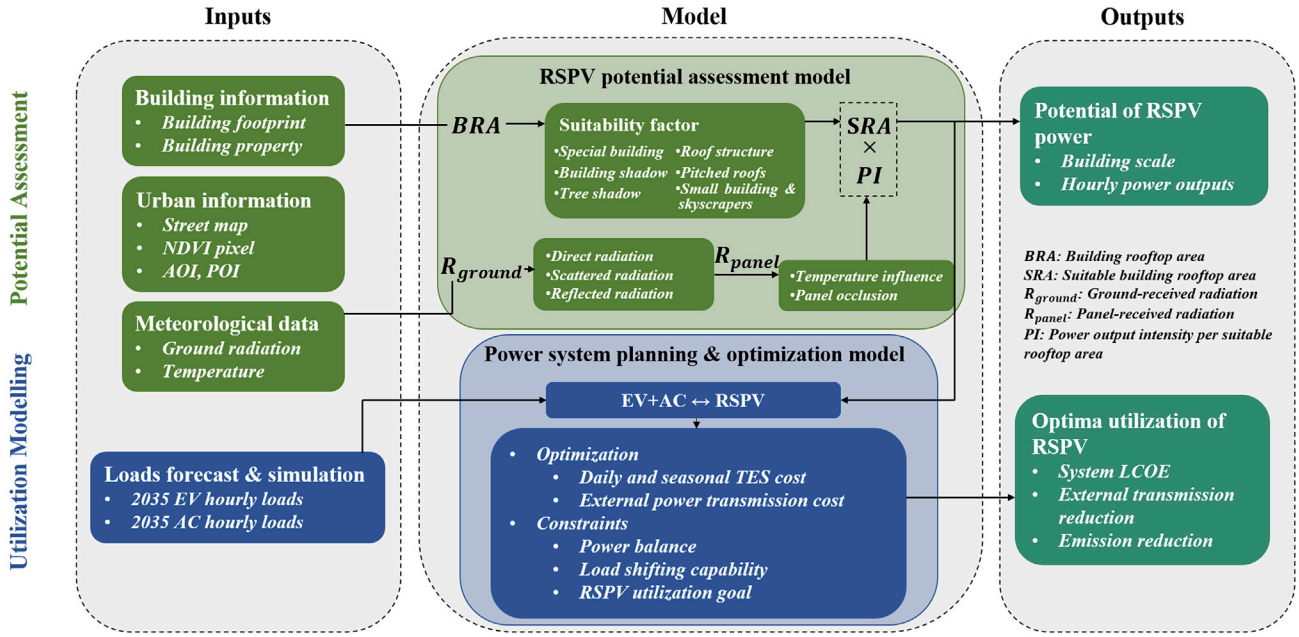

Figure 1. Framework for the potential-utilization linked framework for RSPV in mega-cities

The data inputs in this analysis include geospatial, meteorological, and urban load information. The geospatial data include building footprint, street map, normalized distribution vegetation index (NDVI) pixel, area of interest (AOI), and point of interest (POI) data. (see in STAR Methods and Table S2). The meteorological data include GEOS-5 ground radiation data and temperature data. (see in STAR Methods). The forecasted and simulated 2035 EV and AC hourly loads were derived using the method described in Tables S10 and S11. The RSPV potential assessment model calculated the suitability factors for individual buildings to estimate the suitable rooftop area for the potential RSPV deployment. The RSPV potentials were evaluated as the product of suitable rooftop areas and the power output intensity (PI). Finally, the power system planning & optimization model were applied to calculate the accommodation of RSPV power by emerging EV & AC loads. (STAR Methods).

suitable areas are mainly influenced by building shade and rooftop structure, particularly inside the core Metropolitan (RD2) areas, which are concentrated with a mixture of low-rise buildings and skyscrapers (Figure S4). The capacity potential for RSPV, the potential installed capacity of RSPV on suitable rooftop areas, was estimated at 11.1 GW inside the GM area, approximately 18.3 times the total installed solar PV capacity in the entire Beijing in 2020 (National energy administration, 2021). The corresponding electricity potential, annual electricity generation potential from those RSPV capacities, was estimated at 15.4 TWh, equivalent to 20.8% of the demand for electricity in the GM area or 14.5% in the entire Beijing area in 2019. For daylight hours, from 9 a.m. to 4 p.m., the RSPV power outputs could meet as high as 49.9% of the electric demand in the Beijing GM area. (Table S9).

Results in Figure 2 also suggest that both the capacity and electricity potentials for RSPV in the Beijing GM area increase with a distance from the city center to the suburbs. The capacity potential increases from 0.6 GW inside RD2 to 5.1 GW in the ring area of RD5-RD6, with the corresponding electricity potential increasing from 0.9 TWh to 7.1 TWh. This reflects the fact that for the urban area of Beijing, the further away from the city center, the larger land area and lower plot ratio, which allows, respectively, for greater building rooftop area and better suitability factors for the deployment of solar PV panels. Should the suitability factors of RD5-RD6 hold for the peripheral area, the capacity potential of RSPV outside the RD6 area was estimated at 11.7 GW, bringing a lower boundary of 22.8 GW for the total RSPV capacity in the entire Beijing area. (Figure 2C).

The spatial distribution of the RSPV electricity potential per land-use area and per capita exhibits distinct heterogeneity in the Beijing GM area (see Figures 3A and 3B). The RSPV potential per land area ranges from 0 kWh/m^2 to 35.6 kWh/m^2, with an average value of 7.2 kWh/m^2 (Figure 3A). High values for electricity potential per land-use area are concentrated inside RD4 owing to the high density of buildings. Some hotspots for RSPV potential per land-use area are located within RD5-RD6, such as Shougang Industrial Park at west RD6 and the Yizhuang Development Zone in the southeast RD6 area, reflecting the recent

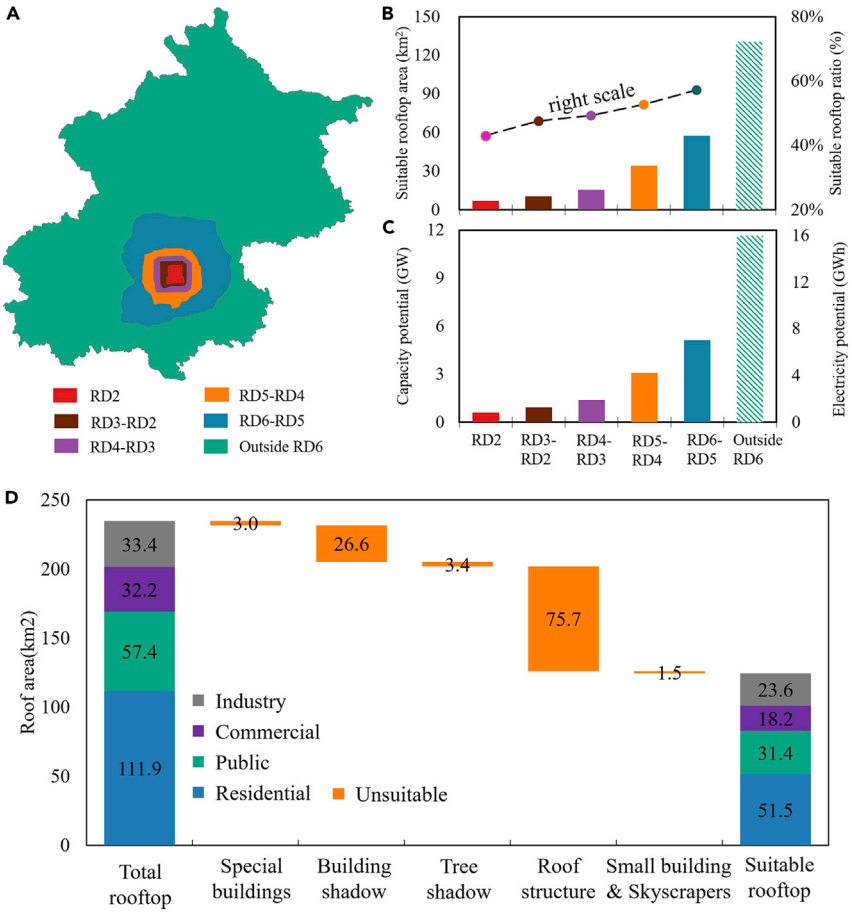

Figure 2. Suitable rooftop area and RSPV potential in different RD locations and kinds of buildings

(A) Visualization of ring road (RD) distribution in Beijing.

(B) Suitable roof area and its ratio in different RDs, the dashed column means the estimated suitable rooftop area outside RD6.

(C and D) Capacity and electricity potential in different RDs, and (D) Impacts of limiting factors on the suitable rooftop areas for RSPV in Beijing Greater Metropolitan area (within sixth ring road, RD6).

urban expansion in Beijing. These areas have developed quite recently and have been concentrated with a number of companies, thus they are mainly occupied by low-rise office buildings and factory buildings with large roof areas. In contrast, the per capita RSPV electricity potential demonstrates a higher value with 1332.4 kWh on average in areas between RD4 and RD6, whereas the values for the area inside RD3 are relatively lower with 728.5 kWh on average. This reflects the trade-off between building and population densities that high population density inside RD3 drives down the per capita RSPV potential, over offsetting the increasing effects from the high building density. As illustrated in Figure 3B, the average value of the per capita RSPV electricity potential amounts to 1030.8 kWh, varying over a wide range from 182.1 kWh to 6543.3 kWh. To put this into context, the average residential power consumption per capita in Beijing was 1168.3 kWh in 2019 (Beijing Municipal Bureau of Statistics, 2021), slightly higher than the average per capita potential for RSPV.

Effective rooftop solar photovoltaics utilization through building-related flexible loads

The opportunities for the utilization of the RSPV potential in the Beijing GM area were further investigated through a power system planning & optimization model to optimize the operation of Beijing's building-related flexible loads including EVs, ACs as well as heat storage from TES (hereafter referred to as the RSPV + system) in 2035 with a minimum cost (see in STAR Methods). As illustrated in Figure 4, results indicate that the 15.4 TWh RSPV from the Beijing GM area could be 100% effectively utilized by loads of EVs and ACs coupled with daily and seasonal TES. The annual load of EVs and ACs in the Beijing GM area are

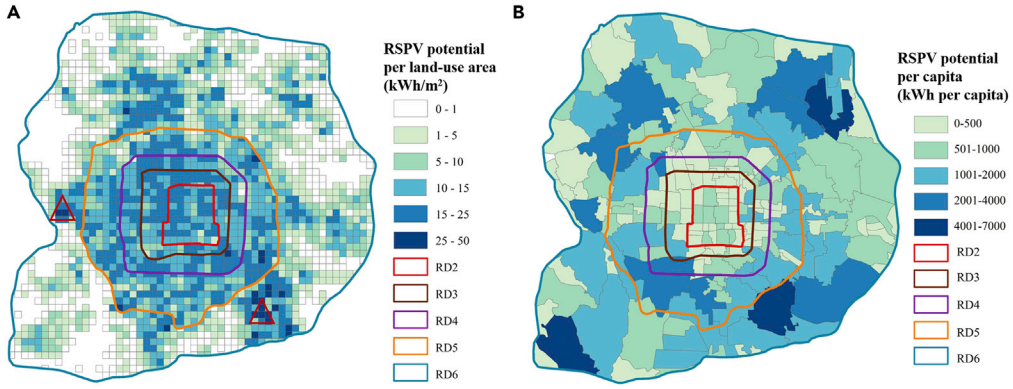

Figure 3. Spatial distribution of RSPV potentials in the Beijing great metropolitan area (RD6)

(A) RSPV electricity potential per land-use area (kWh/m^2/year) inside the RD6 area, with *Shougang Industrial Park and Yizhuang Development Zone are marked with red triangles.*

(B) per capita electricity RSPV potential (kWh per capita) on a subdistrict scale.

projected to increase to 9.9 TWh and 14.3 TWh, respectively, in 2035, which together would raise the consumption ratio of RSPV potential to 61.2% (9.5 TWh) from 27.1% (4.2 TWh) in 2020 without changing their traditional pattern of electricity consumption. About 4.1 TWh electricity from RSPV can be utilized by flexibly running ACs, coupled with the 21.6 GWh daily and 1966.0 GWh seasonal TES capacities including about 0.5 TWh power loss from the TES system (Figure 4). The rest of the RSPV potential (2.8 TWh) can be further accommodated through the smart operation of EVs.

The optimal operation of the RSPV + system demonstrates distinct seasonality in terms of complementary effects (Figure 5). For most cases in summer, the peak of cooling demand is consistent with the peak of RSPV potential and the direct load from EVs and ACs could accommodate more than 95.0% of the RSPV potential (Figures 5E, 5F, 5I, and 5J). The daily TES system works mainly in utilizing RSPV to meet the extremely high demand for cooling through intra-day heating storage, while the seasonal TES system functions as a cooling supplier in early summer (Figures 5H and 5I). The daily and seasonal TES systems together facilitate increasing the ratio of electric cooling fueled by RSPV to total cooling supply from 43.5% to 58.4% in summer. In contrast, the RSPV potential and electric loads from AC heating vary discordantly in winter (Figures 5A and 5B). In this case, the daily TES system is frequently engaged to store heat when RSPV has a surplus relative to the total electric load. During peak-heating hours in winter evenings, the heating demand would be mainly satisfied by the combination of heat supply from daily TES and autumn-stored heat in the seasonal TES system. The daily and seasonal TES systems together increase the ratio of electric heating by RSPV from 30.1% to 77.8% in the total heating supply in winter (Figure 5D). The smart charging of EVs functions to shift the electric load from night to daytime, especially on the days when the RSPV is relatively abundant (Figure 5C). This implies that future EV charging may increasingly rely on public charging near offices to maximally use RSPV. During the Autumn and Spring, the requirement for AC cooling/heating load is reduced to the minimum, and the seasonal TES system stores the surplus RSPV either in the form of cold energy from March 1st to June 15th or heat from September 1st to December 15th (Figures 5m, 5n, 5p, and 5q). In addition, RSPV in Beijing tends to have higher outputs and variations in spring than in autumn, and thus more flexible loads need to be engaged in the former season. The seasonal TES system reaches its full capacity of 1965.9 GWh in spring, in contrast to only 958.6 GWh utilized in autumn. For the same reasons, the percentage of EVs load shifted by the smart charging reaches 39.2% in spring vs. 36.4% in autumn (Figures 5O and 5R).

The RSPV + system would lead to an evident reduction in emissions of CO_2 and three primary criteria air pollutants (NO_x, SO_2, the primary $PM_{2.5}$) by substituting external coal-fired electricity consumed in Beijing delivered from the northern electric power grid. Particularly, the RSPV + system would annually reduce emissions of CO_2 by 16.4 Mt, NO_x by 6.2 kt, SO_2 by 3.0 kt, and the primary $PM_{2.5}$ by 1.3 kt, accounting, respectively, for 19.3%, 6.4%, 19.7% and 4.9% of total emissions in Beijing in 2019.

RSPV + system would not only supply carbon- and pollution-free electric power to Beijing, but also lead to a potentially lower cost for electricity consumption in the future. The overall levelized cost of electricity

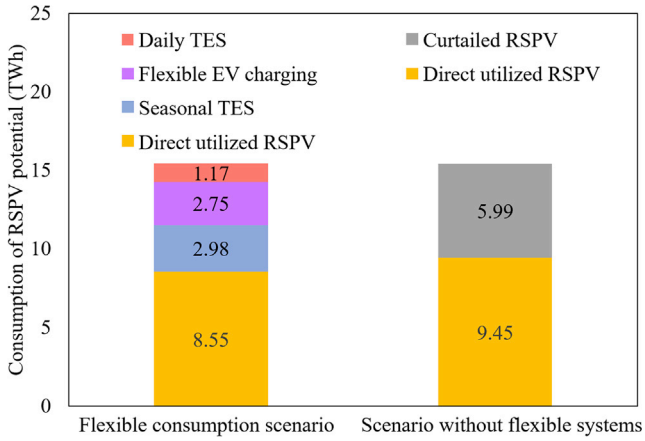

Figure 4. Comparison of annual RSPV consumption between scenario with/without flexible consumption

(LCOE) for RSPV + system in 2035 is estimated at 0.37 (0.32-0.47) RMB/kWh, with breakdowns of 0.17 RMB/kWh (0.15-0.19 RMB/kWh) from the RSPV and 0.20 RMB/kWh (0.17-0.28 RMB/kWh) from the capital expenditure of daily and seasonal TES system. Meanwhile, should 95% of the RSPV potential in the Beijing GM area be utilized (with 5% being curtailed), the cost for RSPV generation would rise to 0.18 RMB/kWh (0.15-0.20 RMB/kWh) but that for TES systems would significantly reduce to 0.13 RMB/kWh (0.11-0.18 RMB/kWh), resulting in an even lower overall LCOE of 0.31 RMB/kWh (0.26-0.38 RMB/kWh).To put this into context, the grid tariff of coal-fired power plants averaged 0.35 RMB/kWh in the northern electric power grid in 2019, which supplied 70% of demand for electricity in Beijing. Additionally, should all increasing electric loads from EVs and ACs in Beijing in 2035 be supplied by external electricity delivered from the northern electric power grid, it would require adding 9.04 GW of new transmission capacity. Utilization of the locally available RSPV power would avoid 8.6 GW external transmission capacity construction (with financial savings of 5.0 billion RMB) to Beijing otherwise required to meet the increasing demand for EVs and ACs.

Discussion and policy implication

This study developed a potential-utilization linked framework for the deployment of RSPV in mega-cities with the consideration of both the tempo-spatial characterization of RSPV resources on the supply side and the optimal accommodation using urban flexible loads on the demand side. We conducted the first of its type of analysis at a megacity scale, taking Beijing as a case in point. Our study demonstrated that approximately 15.4 TWh RSPV is available in the Beijing GM area, and the RSPV potential could be fully accommodated in an environmental-friendly and cost-effective fashion through the optimal operation of increasing electricity loads from EVs and ACs equipped with the TES systems. In addition, the deployment of RSPV + system is expected to reduce the requirements for the construction of a new transmission capacity otherwise required to meet the increasing demand for electricity in Beijing. The methods featured integrative building-scale function identification through multi-source urban information in urban planning, building-scale RSPV suitability analysis in urban geographic analysis, city-scale hourly flexible load quantification in building simulations, and newly developed PSP&O models in electric power system analysis. The results, with building suitability references, high-resolution RSPV potential locations, and local competitive renewable options, are expected to appeal to a broad range of audiences, including not only urban planners and policy makers on civil, grid, and energy systems but also scholars in energy transition, urban geographic analysis, power system planning, climate adaptation, and so forth.

The case study of Beijing may shed light on the opportunities for expanding the application of the "RSPV+" system for the 344 prefectural level cities in China. Through statistical methods based on data derived from the China Urban Construction Statistical Yearbook (Ministry of Housing and Urban-Rural Development of the People's Republic of China, 2021), we estimated a total 531 TWh annual potential of urban RSPV for 344 cities at the prefecture level in the Chinese mainland, which accounts for 7.3% for national total electricity demand in 2020. Given the different RSPV source conditions and urban accommodation capacities, the

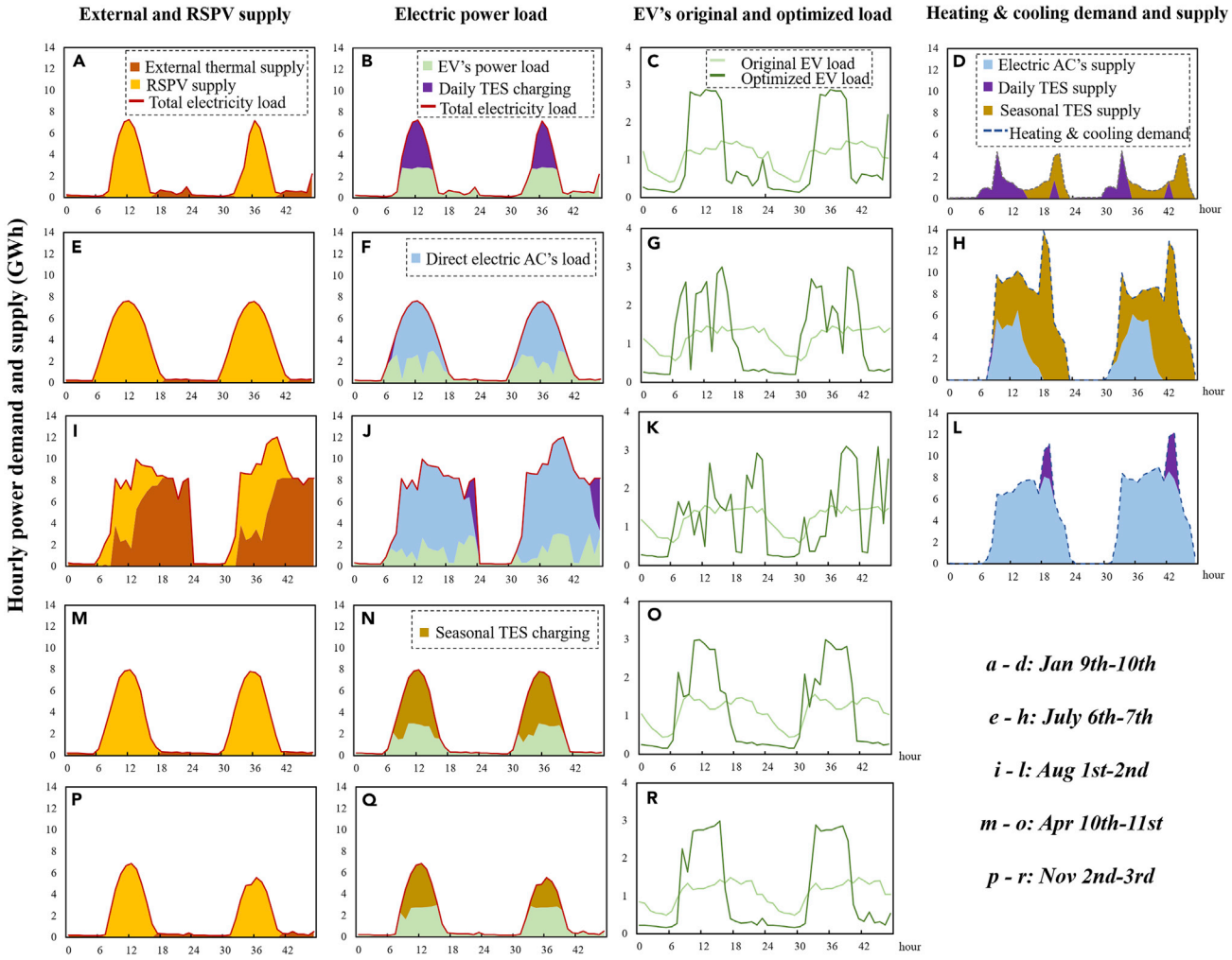

Figure 5. Results of hourly power balance in a two-day cycle for the "RSPV +" system and load optimization for five representative periods in the Beijing GM area

The total load powered by external thermal power and native RSPV (A, E, I, M, and P); load distribution from the power consumption side, which consists of EVs, direct electric ACs, daily TES, and seasonal TES charging (B, F, G, N, and Q); the original and optimized AC and EV loads (C, G, K, O, and R); and dynamic balances between the heating & cooling demand and direct electric ACs, daily TES and seasonal TES (D, H, and I).

optimal operation strategies of the flexible loads and TES system may vary among different cities, and so do the levelized costs of the RSPV + system. In this case, the strategy of the RSPV utilization in different cities should be tailored to their local conditions to maximize their climate and environmental benefit. If such an RSPV + scheme was introduced across China and other megacities globally, the impact would be a massive reduction in greenhouse gas emissions and strongly support carbon neutrality targets.

During the development of RSPV + system, non-residential buildings, especially industry and commercial (I&C) buildings, possess relative advantages over residential buildings. The industry and commercial buildings tend to have larger individual suitable rooftop areas for the deployment of RSPV panels than residential buildings. Especially industrial buildings, they are mainly located in the suburban areas between RD6-RD5 (Figure S7), where buildings have low density and similar height. Therefore, industry buildings are impacted less by building shadows than residential buildings. In addition, I&C buildings possess a relatively large demand for electricity per unit area (Wu, 2017) and their electricity use patterns match well with the diurnal variation of the RSPV power outputs. Thus, the I&C buildings tend to have a higher self-consumption ratio of RSPV electricity, which offsets more usage of high-price electricity from the electric power grid and improves the financial competitiveness of I&C buildings. The higher electricity prices for I&C buildings also consolidate their RSPV economic feasibility. The

Table 1. Roof structure availability for buildings in Beijing

Estimated parameter	Value
Residential, height<15 m	60%
Residential, height>15 m	50%
Public & Commercial, height<15 m	80%
Public & Commercial, height>15 m	60%
Industry	80%

I&C RSPV enjoys higher IRR (8.81%) and shorter DPBP (5.93 years) relative to those for residential RSPV with an IRR of 18.52% and DPBP of 12.32 years (Table S16).

For residential RSPV application, challenges exist in terms of risks of waterproof, fireproof, and regulation violation for aged buildings, which take up 30-50% of residential buildings in mega-cities in China (Wei et al., 2017). However, those barriers could be overcome by renovation programs for old residential communities proposed in the aftermath of COVID-19, which aim at modernizing old residential buildings. In addition, the residential innovation program also allows intelligent transformation for the renovated buildings, which would improve demand-side synergistic effects from ACs and EVs as envisaged in the present analysis. Savings in cost would be realized through incorporating the deployment of RSPV + system with those community-renovation programs, which in turn synergistically brings savings in emissions of CO_2 and air pollutants for mega-cities.

For the application of the flexibility in the "RSPV+" system, opportunity exists as the governmental policies in China administratively and financially encourage the development of EV smart charging (The People's Government of Beijing Municipality, 2022) and TES implementation (National Energy Administration, 2020; Shupeidian.BJX, 2021; Shupeidian.BJX, 2022; North China Energy Regulatory Bureau of National Energy Adiministration of China, 2020). The recent pilot daily and seasonal TES projects have shown great success in terms of both operation and business models in Beijing and its surrounding area, such as the TES heating & cooling project in Fanshan Town in Zhangjiakou, and daily & seasonal TES project in Universal Studios Beijing (Chen et al., 2022). The seasonal TES, which are commonly constructed underground in the urban open and green space, would require an estimated 0.08 m^2 per capita space, which is much smaller than the 37 m^2 per capita open space available in Beijing (Shi, 2020). The daily TES could be placed along with the outdoor unit of air conditioners through retrofitting (Liu et al., 2020). In addition, existing literature also projected that the short-term storage capacities would reach 26 GWh in Beijing in 2035 (Zhuo, 2021) and future high renewable penetrated cities would require long-term storage to store around 3-5% of the city annual electricity demand, which is translated to 6-10 TWh for the Beijing's case (Dowling et al., 2020) and consistent with the results from the present analysis. Meanwhile, the application of TES can not only provide RSPV accommodation capacity for low-carbon heating/cooling but also relieve the burden on the power grid, which is hard to be further expanded in mega-cities, through shifting the electric AC peak loads to support the future increasing power demands. To fully support the application of "RSPV+" system, future policies also need to synergistically incorporate the development of RSPV along with the flexibility sources, such as combining together the current separate financial supports or encouraging third-party on specially owning and operating "RSPV+" system to benefit the effective management.

Limitations of the study

Our results, which imply an annual 15.4 TWh RSPV potential for a year in 2020, may represent a lower boundary of the total RSPV potential for Beijing. First, the building footprints in Beijing were derived from the Web Map system, which could not fully cover some of the low-rise buildings and factory sheds in the suburban area of RD6-RD5. This is also reflected through the comparison with the literature prediction data (Li et al., 2020). Second, the research did not quantify the RSPV potential and utilization in Beijing rural area outside RD6 where RSPV is also expected to expand in the next decades, also locked the RSPV potential until estimated 2020 building stock without considering the future building stock growth until 2035. In addition, demand-side response capacities of other building appliances, such as refrigerators, dishwashers, or laundry machines, were not considered in this study, which may further improve the utilization of RSPV and relieve the required flexibility of EVs and ACs. Potentially interesting

research should incorporate a more detailed classification of building the property and other sources of demand response capability, to completely depict the opportunities for RSPV application in urban areas. Meanwhile, the penetration of RSPV would also probably reshape the electricity market, and even the users' incentive to engage in the RSPV accommodation. The adoption dynamics from the perspective of consumers could be included in future research to systematically address the RSPV opportunity in the longer term.

STAR★METHODS

Detailed methods are provided in the online version of this paper and include the following:

- KEY RESOURCES TABLE
- RESOURCE AVAILABILITY
  - Lead contact
  - Materials availability
  - Data and code availability
- METHODS DETAILS
  - Suitable rooftop area
- TECHNICAL POTENTIAL
  - PV panel density
  - Panel-received radiation
  - Temperature influence
  - Hourly power outputs
- POWER SYSTEM PLANNING & OPTIMIZATION MODEL FOR THE RSPV + SYSTEM

SUPPLEMENTAL INFORMATION

Supplemental information can be found online at https://doi.org/10.1016/j.isci.2022.104890.

ACKNOWLEDGMENTS

This work was supported by the National Natural Science Foundation of China (No. 72025401, 71722003, 71974108, and 71690244), Tsinghua University-INDITEX Sustainable Development Fund.

AUTHOR CONTRIBUTIONS

Conceptualization, M.S., X.L., and A.F.; Methodology, M.S., H.J., S.C., N.Z., and Y.W.; Investigation, M.S. and Q.M.; Writing – Original Draft, M.S.; Writing – Review & Editing, X.L., A.F., and R.F.

DECLARATION OF INTERESTS

The authors declare that they have no known competing financial interests or personal relationships that could have appeared to influence the work reported in this article.

Received: February 14, 2022
Revised: July 20, 2022
Accepted: August 3, 2022
Published: September 16, 2022

SUPPORTING CITATIONS

The following references appear in the Supplemental information: Abu-Hamdeh and Taherian, 2015, Anjuke, 2022, Author Anonymous, 2020, Dulac and Hu, 2019, Fan et al., 2015, Huang, 2013, Li, 2007, Long, 2016, Lu et al., 2021, National Statistics Bureau, 2019, National Statistics Bureau, 2020, Novo et al., 2010, Quan, 2020, Rashedi and Khanam, 2020, Renaldi and Friedrich, 2017, Stamford and Azapagic, 2018, Tang et al., 2019, Wang et al., 2018, Wei et al., 2021, Wei, 2020, Xue et al., 2019, Yan et al., 2019, Zhang, 2014, Zhuo et al., 2020.

REFERENCES

Abu-Hamdeh, O., and Taherian, H. (2015). Optimization of distributed power generation system components for a residential building. ASHRAE Annual Conference 2015, ASHRAE Transactions, *121*.

Author Anonymous. (2020). Detailed information of the cost of distributed photovoltaic power plants. Chinese. Guangfu.BJX. https://guangfu.bjx.com.cn/news/20180126/876974.shtml.

Anjuke., 2022. Anjuke real estate information service platform. (www.anjuke.com).

Baidu Map Open Platform., 2022. (https://api.map.baidu.com/lbsapi).

Beijing Municipal Bureau of Urban Planning (2012). Design Code for Solar Photovoltaic System of Civil Buildings (Beijing Municipal Bureau of Urban Planning, Beijing Municipal Bureau of Quality and Technical Supervision).

Bergamasco, L., and Asinari, P. (2011). Scalable methodology for the photovoltaic solar energy potential assessment based on available roof surface area: further improvements by ortho-image analysis and application to Turin (Italy). Sol. Energy *85*, 2741–2756.

Bódis, K., Kougias, I., Jäger-Waldau, A., Taylor, N., and Szabó, S. (2019). A high-resolution geospatial assessment of the rooftop solar photovoltaic potential in the European Union. Renew. Sustain. Energy Rev. *114*, 109309. https://doi.org/10.1016/j.rser.2019.109309.

British Petroleum (2020). Statistical review of world energy 2020. https://www.bp.com/content/dam/bp/business-sites/en/global/corporate/pdfs/energy-economics/statistical-review/bp-stats-review-2020-co2-emissions.pdf.

Byrne, J., Taminiau, J., Kurdgelashvili, L., and Kim, K.N. (2015). A review of the solar city concept and methods to assess rooftop solar electric potential, with an illustrative application to the city of Seoul. Renew. Sustain. Energy Rev. *41*, 830–844.

Beijing Municipal Bureau of Statistics (2021). Beijing Statistics Yearbook 2020.

Cao, L., Dai, J., Pang, Y., Zhao, B., Xu, J., and Li, Z. (2014). Estimation of urban building rooftop-received solar energy by LiDAR and irradiation model in the urban vegetation shading environment. Sci. Silvae Sin. *50*, 99–110. [Chinese].

Chen, S., Lu, X., Miao, Y., Deng, Y., Nielsen, C.P., Elbot, N., Wang, Y., Logan, K.G., McElroy, M.B., and Hao, J. (2019). The potential of photovoltaics to power the belt and road initiative. Joule *3*, 1895–1912.

Chen, H., et al. (2022). Research progress of energy storage technology in China in 2021. Energy Storage Science and Technology *11*, 1052–1076. https://doi.org/10.19799/j.cnki.2095-4239.2022.0105.

Chuneng.BJX (2021). "4.16" Beijing Dahongmen Energy Storage Power Station Fire and Explosion Investigation Results Announced. Chinese. CHUNENG.BJX.com. https://chuneng.bjx.com.cn/news/20211123/1189510.shtml.

China Urban Energy Report Research Group (2019). China Urban Energy Report (China Electric Power Press).

Defaix, P., Van Sark, W., Worrell, E., and de Visser, E. (2012). Technical potential for photovoltaics on buildings in the EU-27. Sol. Energy *86*, 2644–2653.

Denholm, P., Margolis, R.M., Ong, S., and Roberts, B. (2009). Break-even Cost for Residential Photovoltaics in the United States: Key Drivers and Sensitivities (National Renewable Energy Lab).

Dimitriadis, P. (2015). Effects of Overvoltage on Power Consumption (Brunel University London (Brunel University).

Dowling, J.A., Rinaldi, K.Z., Ruggles, T.H., Davis, S.J., Yuan, M., Tong, F., Lewis, N.S., and Caldeira, K. (2020). Role of long-duration energy storage in variable renewable electricity systems. Joule *4*, 1907–1928. https://doi.org/10.1016/j.joule.2020.07.007.

Dulac, J., and Hu, S. (2019). The Future of Cooling in China: Delivering on Action Plans for Sustainable Air Conditioning (International Energy Agency, Tsinghua University Building Energy Research Center).

Fan, S.B., Tian, L.d., Zhang, D.x., and Qu, S. (2015). Emission factors of vehicle exhaust in Beijing. Environ. Sci. J. Integr. Environ. Res. *36*, 2374–2380. [Chinese].

Fogl, M., and Moudrý, V. (2016). Influence of vegetation canopies on solar potential in urban environments. Appl. Geogr. *66*, 73–80.

Folsom. (2013). Demand Response and Energy Efficiency Roadmap: Maximizing Preferred Resources (California Independent System Operator).

Unión Española Fotovoltaica (2018). Spain removes controversial sun tax. https://www.solarpowereurope.org/spain-removes-controversial-sun-tax/.

Gagnon, P., Margolis, R., Melius, J., Phillips, C., and Elmore, R. (2016). Rooftop Solar Photovoltaic Technical Potential in the United States. A Detailed Assessment Technical Report NREL/TP-6A20-65298 (National Renewable Energy Lab).

Ghosh, S., Vale, R., and Vale, B. (2006). Domestic energy sustainability of different urban residential patterns: a New Zealand approach. Int. J. Sustain. Dev. World Ecol. *9*, 16–37.

Good, C., Shepero, M., Munkhammar, J., and Boström, T. (2019). Scenario-based modelling of the potential for solar energy charging of electric vehicles in two Scandinavian cities. Energy *168*, 111–125. https://doi.org/10.1016/j.energy.2018.11.050.

Gorelick, N., Hancher, M., Dixon, M., Ilyushchenko, S., Thau, D., and Moore, R. (2017). Google earth engine: planetary-scale geospatial analysis for everyone. Remote Sens. Environ. *202*, 18–27.

Guo, X.L. (2015). Rooftop Solar PV Potential Assessment of Xuzhou Based on Roof Area (China University of Mining & Technology). [Chinese].

Huang, Jian, et al. (2013). Study on Energy Conservation Potential and Promotion Mechanism for Civil Buildings in Beijing (Energy Foundation China). [Chinese].

International renewable energy agency (2021). Renewable Energy Capacity Ststistics 2020 (International renewable energy agency).

Izquierdo, S., Rodrigues, M., and Fueyo, N. (2008). A method for estimating the geographical distribution of the available roof surface area for large-scale photovoltaic energy-potential evaluations. Sol. Energy *82*, 929–939.

Jacobson, M.Z., and Jadhav, V. (2018). World estimates of PV optimal tilt angles and ratios of sunlight incident upon tilted and tracked PV panels relative to horizontal panels. Sol. Energy *169*, 55–66.

Joshi, S., Mittal, S., Holloway, P., Shukla, P.R., Ó Gallachóir, B., and Glynn, J. (2021). High resolution global spatiotemporal assessment of rooftop solar photovoltaics potential for renewable electricity generation. Nat. Commun. *12*, 5738. https://doi.org/10.1038/s41467-021-25720-2.

Joskow, P.L. (2018). Challenges for Wholesale Electricity Markets with Intermittent Renewable Generation at Scale: The U.S. Experience (MIT Center for Energy and Environmental Policy Research).

Mansouri Kouhestani, F., Byrne, J., Johnson, D., Spencer, L., Hazendonk, P., and Brown, B. (2019). Evaluating solar energy technical and economic potential on rooftops in an urban setting: the city of Lethbridge, Canada. Int. J. Energy Environ. Eng. *10*, 13–32.

Laine, H.S., Salpakari, J., Looney, E.E., Savin, H., Peters, I.M., and Buonassisi, T. (2019). Meeting global cooling demand with photovoltaics during the 21st century. Energy Environ. Sci. *12*, 2706–2716. https://doi.org/10.1039/C9EE00002J.

Lee, M., Hong, T., Jeong, K., and Kim, J. (2018). A bottom-up approach for estimating the economic potential of the rooftop solar photovoltaic system considering the spatial and temporal diversity. Appl. Energy *232*, 640–656.

Levinson, R., Akbari, H., Pomerantz, M., and Gupta, S. (2009). Solar access of residential rooftops in four California cities. Sol. Energy *83*, 2120–2135.

Li, D., Liu, G., and Liao, S. (2015). Solar potential in urban residential buildings. Sol. Energy *111*, 225–235.

Li, M., Koks, E., Taubenböck, H., and van Vliet, J. (2020). Continental-scale mapping and analysis of 3D building structure. Rem. Sens. Environ. *245*, 111859. https://doi.org/10.1016/j.rse.2020.111859.

Li, Z.J. (2007). Study on the Life Cycle Consumption of Energy and Resource of Air Conditioning in Urban Residential Buildings in China (Tsinghua Univercity). [Chinese].

Litjens, G.B.M.A., Kausika, B., Worrell, E., and van Sark, W. (2018). A spatio-temporal city-scale assessment of residential photovoltaic power integration scenarios. Sol. Energy *174*, 1185–1197. https://doi.org/10.1016/j.solener.2018.09.055.

Liu, Y., Liu, T., Ji, B., and Wang, B. (2020). An economic evaluation of refrigeration and air-conditioning system retrofit in large-scale public buildings: a case study of Beijing Capital International Airport Terminals. J. Clean. Prod. *245*, 118934.

Liu, X.Y. (2011). Architectural and livable forms differences between North and south China. Architect. Des *10*, 200–201. [Chinese].

Long, Y. (2016). Redefining Chinese city system with emerging new data. Appl. Geogr. *75*, 36–48.

LONGi. (2021). Hi-MO 4m LR4-60HPH Specification Table. Chinese. https://www.longi-solar.com/uploadfile/default/2021/05/20210512115417137.pdf.

Lu, X., Chen, S., Nielsen, C.P., Zhang, C., Li, J., Xu, H., Wu, Y., Wang, S., Song, F., Wei, C., et al. (2021). Combined solar power and storage as cost-competitive and grid-compatible supply for China's future carbon-neutral electricity system. Proc. Natl. Acad. Sci. USA *118*, e2103471118. https://doi.org/10.1073/pnas.2103471118.

Lucchesi, R. (2017). File Specification for GEOS-5 FP, *4* (GMAO Office Note No), 1.1 Version. https://gmao.gsfc.nasa.gov/pubs/docs/Lucchesi1202.pdf.

ESCN (2021). Main Points of Fire Protection Design of Pre-packed Box-type Lithium Iron Phosphate Battery Energy Storage Power Station (ESCN). [Chinese]. http://escn.com.cn/news/show-1237753.html.

Martin, H., Buffat, R., Bucher, D., Hamper, J., and Raubal, M. (2022). Using rooftop photovoltaic generation to cover individual electric vehicle demand—a detailed case study. Renew. Sustain. Energy Rev. *157*, 111969. https://doi.org/10.1016/j.rser.2021.111969.

Masters, G. (2005). Renewable and Efficient Electric Power Systems (John Wiley & Sons, Inc).

Ministry of Housing and Urban-Rural Development of the People's Republic of China (2021). China Urban Construction Statictical Yearbook (China Statistics Press).

Mohajeri, N., Assouline, D., Guiboud, B., Bill, A., Gudmundsson, A., and Scartezzini, J.L. (2018). A city-scale roof shape classification using machine learning for solar energy applications. Renew. Energy *121*, 81–93. https://doi.org/10.1016/j.renene.2017.12.096.

Beijing Municipal Bureau of Statistics (2018). Beijing First Municipal Geoinformation Survey (Beijing Municipal Commission of Planning and Natural Resources, Beijing Municipal Bureau of Statistics). [Chinese].

National Energy Administration (2020). Reply to recommendation No. 9178 of the third session of the thirteenth national People's congress. [Chinese]. http://zfxxgk.nea.gov.cn/2020-09/09/c_139419445.htm.

National energy administration (2021). 2013-2020 Photovoltaic Power Statistics.

National Statistics Bureau. (2019). China Statistical Yearbook (China Statistics Press). [Chinese].

National Statistics Bureau (2020). China Statiscal Yearbook on Construction (China Statistics Press). Chinese.

North China Energy Regulatory Bureau of National Energy Adiministration of China (2020). Notice of the north China energy regulatory Bureau on continuing the pilot work of third-party independent entities to participate in the north China auxiliary service market. [Chinese]. http://hbj.nea.gov.cn/adminContent/initViewContent.do?pk=00000000764722690176 4c4e28ae0011.

Novo, A.V., Bayon, J.R., Castro-Fresno, D., and Rodriguez-Hernandez, J. (2010). Review of seasonal heat storage in large basins: water tanks and gravel-water pits. Appl. Energy *87*, 390–397.

Obi, M., and Bass, R. (2016). Trends and challenges of grid-connected photovoltaic systems - a review. Renew. Sustain. Energy Rev. *58*, 1082–1094.

Ordóñez, J., Jadraque, E., Alegre, J., and Martínez, G. (2010). Analysis of the photovoltaic solar energy capacity of residential rooftops in Andalusia (Spain). Renew. Sustain. Energy Rev. *14*, 2122–2130.

Peng, J., and Lu, L. (2013). Investigation on the development potential of rooftop PV system in Hong Kong and its environmental benefits. Renew. Sustain. Energy Rev. *27*, 149–162.

Quan, Yongshen, et al. (2020). 2019 Beijing Transport Annual Report (Beijing Transport Institute). [Chinese].

Rashedi, A., and Khanam, T. (2020). Life cycle assessment of most widely adopted solar photovoltaic energy technologies by mid-point and end-point indicators of ReCiPe method. Environ. Sci. Pollut. Res. Int. *27*, 29075–29090. https://doi.org/10.1007/s11356-020-09194-1.

Renaldi, R., and Friedrich, D. (2017). Multiple time grids in operational optimisation of energy systems with short- and long-term thermal energy storage. Energy *133*, 784–795.

Saxena, S., MacDonald, J., Black, D., and Kiliccote, S. (2015). Quantifying the flexibility for electric vehicles to offer demand response to reduce grid impacts without compromising individual driver mobility needs. SAE International.

Schallenberg-Rodríguez, J. (2013). Photovoltaic techno-economical potential on roofs in regions and islands: the case of the Canary Islands. Methodological review and methodology proposal. Renew. Sustain. Energy Rev. *20*, 219–239.

Sharma, V., Aziz, S.M., Haque, M.H., and Kauschke, T. (2020). Effects of high solar photovoltaic penetration on distribution feeders and the economic impact. Renew. Sustain. Energy Rev. *131*, 110021. https://doi.org/10.1016/j.rser.2020.110021.

Shen, H., Chu, Y.F., et al. (2013). Solar Photovoltaic Architectural Design: Application of Photovoltaic Power Generation in Old Buildings Urban Areas and Scenic Spots (Science Press). [Chinese].

Shepero, M., Lingfors, D., Widén, J., Bright, J.M., and Munkhammar, J. (2020). Estimating the spatiotemporal potential of self-consuming photovoltaic energy to charge electric vehicles in rural and urban Nordic areas. J. Renew. Sustain. Energy *12*, 046301.

Sieverts, T. (2003). Cities without Cities: An Interpretation of the Zwischenstadt, 1st edition (Routledge). https://doi.org/10.4324/9780203380581.

Singh, R., and Banerjee, R. (2015). Estimation of rooftop solar photovoltaic potential of a city. Sol. Energy *115*, 589–602.

Song, X., Huang, Y., Zhao, C., Liu, Y., Lu, Y., Chang, Y., and Yang, J. (2018). An approach for estimating solar photovoltaic potential based on rooftop retrieval from remote sensing images. Energies *11*, 3172.

Stamford, L., and Azapagic, A. (2018). Environmental impacts of photovoltaics: the effects of technological improvements and transfer of manufacturing from Europe to China. Energy Technol. *6*, 1148–1160. https://doi.org/10.1002/ente.201800037.

Shupeidian.BJX (2022). State Grid Integrated Energy Service Group's Virtual Power Plant Participates in Peak Regulation of Power Grid Auxiliary Services Market. Chinese. SHUPEIDIAN.BJX.COM. https://shupeidian.bjx.com.cn/html/20220107/1198079.shtml.

Shi, Weiliang, et al. (2020). Beijing Green&open Space System Planning (Beijing Municipan Insititute of City Planning&Design). [Chinese]. http://ghzrzyw.beijing.gov.cn/zhengwuxinxi/ghcg/zxgh/201912/P020191213628223194729.pdf.

Shupeidian.BJX (2021). Xiongan Virtual Power Plant Operation Platform Is Deployed Online. Chinese. SHUPEIDIAN.BJX.COM. https://shupeidian.bjx.com.cn/html/20211223/1195396.shtml.

Tang, L., Qu, J., Mi, Z., Bo, X., Chang, X., Anadon, L.D., Wang, S., Xue, X., Li, S., Wang, X., and Zhao, X. (2019). Substantial emission reductions from Chinese power plants after the introduction of ultra-low emissions standards. Nat. Energy *4*, 929–938. https://doi.org/10.1038/s41560-019-0468-1.

The People's Government of Beijing Municipality (2013). Beijing Clean Air Act Plan 2013-2017 (Beijing Municipal Ecology and Environment Bureau). [Chinese].

The People's Government of Beijing Municipality (2020). Breakdown List of Sustainability Commitments for the Beijing 2022 Winter Olympics and Paralympics (Beijing Municipal Comission of Development and Reform, Beijing Municipal Finance Bureau, Beijing Municipal Commision of Housing and Urban-rural Development).

The people's government of Beijing Municipality (2022). The urban management and development plan of Beijing during the "14th Five-Year Plan"

period. http://www.beijing.gov.cn/zhengce/zhengcefagui/202204/t20220412_2672524.html.

Tooke, T.R., Coops, N.C., Voogt, J.A., and Meitner, M.J. (2011). Tree structure influences on rooftop-received solar radiation. Landsc. Urban Plan. *102*, 73–81.

Vardimon, R. (2011). Assessment of the potential for distributed photovoltaic electricity production in Israel. Renew. Energy *36*, 591–594.

Walker, A. (2017). PV O&M Cost Model and Cost Reduction (Golden, CO (United States): National Renewable Energy Lab.(NREL)). No. NREL/PR-7A40-68023.

Wang, Zhongying, et al. (2019). China PV Development Outlook in 2050 (Energy Research Institute NDRC & Longi Green Technology CO.Ltd). Chinese.

Wang, J., Wang, R., Zhu, Y., and Li, J. (2018). Life cycle assessment and environmental cost accounting of coal-fired power generation in China. Energy Pol. *115*, 374–384. https://doi.org/10.1016/j.enpol.2018.01.040.

Wei, W., Li, J., Chen, B., Wang, M., Zhang, P., Guan, D., Meng, J., Qian, H., Cheng, Y., Kang, C., et al. (2021). Embodied greenhouse gas emissions from building China's large-scale power transmission infrastructure. Nat. Sustain. *4*, 739–747. https://doi.org/10.1038/s41893-021-00704-8.

Wei, et al. (2017). Beike Insititute in Chinese. http://admin.fangchan.com/uploadfile/uploadfile/annex/1/1875/5ed0ec6fbb537.pdf.

Wei, Y.X. (2020). The Second Revolution in the Housing Sector (Beike Research Insititute). Chinese.

Wiginton, L.K., Nguyen, H.T., and Pearce, J.M. (2010). Quantifying rooftop solar photovoltaic potential for regional renewable energy policy. Comput. Environ. Urban Syst. *34*, 345–357.

World Resource Insititute (2020). STATEMENT: China commits to stronger climate targets at climate ambition summit. https://www.wri.org/news/2020/12/statement-china-commits-stronger-climate-targets-climate-ambition-summit.

Wu, Yong, et al. (2017). China Building Energy Consumption Research Report (Energy Foundation China). Chinese.

Xue, L., et al. (2019). Quantifying the Grid Impacts from Large Adoption of Eletric Vehicles in China (World Resource Institute). [Chinese].

Yan, J., Yang, Y., Elia Campana, P., and He, J. (2019). City-level analysis of subsidy-free solar photovoltaic electricity price, profits and grid parity in China. Nat. Energy *4*, 709–717. https://doi.org/10.1038/s41560-019-0441-z.

Yang, T., Liu, W., Kramer, G.J., and Sun, Q. (2021). Seasonal thermal energy storage: a techno-economic literature review. Renew. Sustain. Energy Rev. *139*, 110732.

Zhang, S.J. (2014). Characteristics and Emission Control Strategies of Vehicle Emissions in Typical Cities of China (Tsinghua University). Chinese.

Zhang, H. (2017). Research on PV Energy Potential of Rooftop in Urban Area (Tianjin University). [Chinese].

Zhong, T., Zhang, Z., Chen, M., Zhang, K., Zhou, Z., Zhu, R., Wang, Y., Lü, G., and Yan, J. (2021). A city-scale estimation of rooftop solar photovoltaic potential based on deep learning. Appl. Energy *298*, 117132. https://doi.org/10.1016/j.apenergy.2021.117132.

Zhuo, Zhenyu, et al. (2021). Cost Increments of Electricity Supply to Achieve Carbon Neutrality in China (Nature Communication).

Zhuo, Z., Zhang, N., Yang, J., Kang, C., Smith, C., O'Malley, M.J., and Kroposki, B. (2020). Transmission expansion planning test system for AC/DC hybrid grid with high variable renewable energy penetration. IEEE Trans. Power Syst. *35*, 2597–2608.

STAR★METHODS

KEY RESOURCES TABLE

REAGENT or RESOURCE	SOURCE	IDENTIFIER
Deposited data		
Building scale RSPV potential in Beijing GM area	This study	N/A
Software and algorithms		
ArcGIS 10.5	Environmental Systems Research Institute	https://www.arcgis.com/
Optimization algorithm	This study	See STAR Methods and supplemental information
MATLAB	MathWork	https://ww2.mathworks.cn/products/matlab.html
CPLEX Optimization Studio 12.5.1	IBM (International Business Machines Corporation) support	https://www.ibm.com/support/pages/downloading-ibm-ilog-cplex-optimization-studio-1251

RESOURCE AVAILABILITY

Lead contact

Further information and requests for resources should be directed to and will be fulfilled by the lead contact, Xi Lu (xilu@tsinghua.edu.cn).

Materials availability

This study did not generate new unique materials.

Data and code availability

The datasets generated in this study are available from the lead contact on reasonable request.

METHODS DETAILS

Suitable rooftop area

The suitable area (A_{sui}) for the deployment of RSPV can be estimated using Equation 1:

$$A_{sui} = \left(A_{total} - A_{spe} - A_{bs}\right) \times F_{bs} \times F_{ts} \times F_{rs} \times F_{tilt} - A_{sma} \quad \text{(Equation 1)}$$

where A_{total} refers to the total rooftop area, A_{spe} indicates the inapplicable area of buildings with historic or ornamental value, A_{bs} indicates the unsuitable rooftop area due to building shadow, F_{bs} is the dynamic building shadow coefficient on the suitable area, F_{ts} and F_{rs} indicate the area restriction factors from tree shadow and roof structure, respectively, and A_{sma} is the unsuitable small building area.

Special buildings

Special buildings symbolize the historical inheritance of a city, which has cultural and historical significance. Although European architects have had some experience with historical buildings and RSPV integration (Shen and Chu, 2013), rooftop construction on special buildings is regarded subject to high risks in China (Zhang, 2017), and these buildings were considered unsuitable for solar PV installation in this analysis. Areas with special buildings (A_{spe}) can be identified through the scenic landmarks in areas of interest (AOI) data from Baidu maps (Baidu Map Open, 2022).

Building shadow

The building shadow effect is an important limiting factor for RSPV deployment in urban areas, reflecting the phenomenon that high-rise buildings obstruct light to adjacent low-rise buildings. Following Gagnon et al. (2016), this analysis adopted a Hillshade modeling method to quantify the influence of building shadows using the building footprint polygon data derived from the Baidu map system. The method uses elevation information raster data, combined with solar azimuth and solar altitude at different hours, to generate a 1m*1m greyscale pixel map with values ranging from 0 (shadow) to 255 (highest normal-beam solar radiation). The greyscale for the rooftop area can be indexed by properly setting the size of the elementary cells of the raster data during conversion from the building footprint polygon data.

Seasonal variation was captured by running the simulation hourly from 8 a.m. to 4 p.m. every 15th day in the 12 months, which resulted in 108 pieces of shadow raster layers. At each hour, if the greyscale of a raster cell is lower than the maximum greyscale value on a horizontal surface for that hour in the same location, the cell is regarded as "shaded", and the value of its effective sunlight hour is set as zero; otherwise, the value set as one. Following this rule, the 108 layers of greyscale values were converted into effective sunlight hours, the sum of which was divided by 12 to derive the daily average values. Then, we adopted the threshold suggested by the U.S. National Renewable Energy Laboratory (NREL), which requires effective rooftop areas with no less than 5 h of average daily effective sunlight (Gagnon et al., 2016). The rooftop areas below this threshold were regarded as ineffective, as indicated by A_{bs}. In addition, an hourly dynamic factor, F_{bs}, was defined by the ratio of dynamically unshaded raster cells to total cells in the identified effective sunlit areas (i.e., the total surface area excluding A_{bs}).

Tree shadow

Tree shadow is another major source of urban rooftop shade. In this study, buildings covered by tree shadows were required to meet two criteria: (1) their layouts intersect with the buffer zones of trees, and (2) their heights are lower than those of trees. For buildings identified as under the influence of tree shadow, we introduced an intensity index ($I_{tree} = NDVI/H$) to measure the influence. *NDVI* refers to the normalized distribution vegetation index, which was derived from satellite Landsat data in 30m resolution (Gorelick et al., 2017), and *H* denotes the height of the buildings. We further assumed that the shadow influence factor (F_{ts}) was linearly proportional to the intensity index (I_{tree}). For the case study of Beijing, F_{ts} was assumed to range from 8 to 40%, as reported in previous studies based on direct LIDAR detection sampling (Fogl and Moudrý, 2016; Levinson et al., 2009; Tooke et al., 2011; Cao et al., 2014).

Roof structure

The roof structure factor refers to the influence of roof facilities on the installation and generation of RSPV systems, including elevators, parapets, water tanks, ventilation shafts and green roofs. Due to the complexity of roof structures, existing studies have assigned parameters to quantify architectural suitability based on rooftop classification (Byrne et al., 2015; Bergamasco and Asinari, 2011; Peng and Lu, 2013; Zhang, 2017; Schallenberg-Rodriguez, 2013). Following the parameter assignment in a study by Zhang (2017) on Tianjin, a mega city near Beijing, this study also distinguished the roof structure factors for individual buildings in Beijing by their type and height (Table 1). We introduced a six-step method to define individual building properties into four types (residential, public, commercial and industry) using a series of urban planning data (Detail in Table S3). The heights of buildings were derived from building footprint data.

Pitched roofs, small buildings and skyscrapers

The slope of pitched roofs is also an important factor affecting roof availability for the installation of solar PV panels. A fixed tilt and southward orientation are commonly selected for flat roofs, while along-the-roof installation is best for pitched roofs. Here, we assume all buildings with flat roofs for the three reasons: (1) from the history of architecture in northern China (Liu, 2011) and sample rooftop investigations (Song et al., 2018), pitched rooftop buildings account for a low percentage among all buildings in Beijing, (2) the difference in the panel-received radiation per horizontal projected rooftop area is estimated within 5% between the flat and pitched roofs in Beijing, and (3) buildings with pitched roofs are generally low-rise and relatively small, the suitable roof areas from pitched roofs are negligible due to exclusion by the combination of roof properties, building shadow and suitable area limits (>33 m^2) (Lee et al., 2018). Meanwhile, we also excluded the skyscrapers (taller than 90m) as the unsuitable building due to their sophisticated rooftop shape, which may not accommodate the RSPV.

TECHNICAL POTENTIAL

The technical parameters pertaining to power outputs from the RSPV system include PV panel density, the impact of temperature on PV efficiency, and shading effects between panels.

PV panel density

In this analysis, we assume that all PV panels are installed southward in transverse layouts. The density of PV panels was determined to ensure that there was no obstruction between PV modules between 9 a.m. and 3

p.m. on the winter solstice (Beijing Municipal Bureau of Urban Planning, 2012). Thus, the module space, d, and the utilization rate of roof, RF_{ratio}, can be calculated by Equation 2 and Equation 3.

$$d = l \times \cos\theta + l \times \frac{\sin\theta \times \cos\alpha_n}{\tanh_n} \quad \text{(Equation 2)}$$

$$RF_{ratio} = \frac{1}{\cos\theta + \frac{\sin\theta}{\tanh_n} \times \cos\alpha_n} \quad \text{(Equation 3)}$$

where d is the module space, l is the module length, θ is the installation tilt angle, α_n and h_n are the solar azimuth and solar altitude at 9 a.m. or 3 p.m. during the winter solstice, and RF_{ratio} is the roof coverage ratio. Based on parameters selected for projects in practice (Jacobson and Jadhav, 2018), the optimal value of θ was selected as 35° in the case study of Beijing.

The shadow areas from panel occlusion SHD_{PV} vary hourly and can be calculated as follows:

$$M = l \times \frac{\sin\theta \times \cos\alpha}{\tanh} \quad \text{(Equation 4)}$$

$$m = d - l \times \cos\theta \quad \text{(Equation 5)}$$

$$H_{SP} = \arctan\left(\frac{\tanh}{\cos\alpha}\right) \quad \text{(Equation 6)}$$

$$SHD_{PV} = \frac{(M - m)}{l} \times \frac{\sin H_{SP}}{\sin(\pi - H_{SP} - \theta)} \quad \text{(Equation 7)}$$

where M is the length difference between the south-projection direction and the vertical projection of the PV panel, m is the length difference between the module space, and H_{SP} is the projection of the solar elevation angle in the south direction.

Panel occlusion has evident effects on the power outputs of solar PV systems due to the short circuit effect inside the panel, as shade on a small part of the panel may interfere with the power output due to series cell connections and hotspot effects (Chen et al., 2019). The relationship between the power loss F_{PVSHD} and SHD_{PV} can be calculated by Equation 8.

$$F_{PVSHD} = 1 - (\text{floor}(SHD_{PV} \times 6) + 1) \times 1/6 \quad \text{(Equation 8)}$$

Panel-received radiation

The radiation intercepted by PV panels consists of three parts: directed tilt radiation (I_{DT}, W/m^2), scattered tilt radiation (I_{SH}, W/m^2) and reflected tilted radiation (I_{RT}, W/m^2). Through the method introduced by Masters (2005), those three streams of radiation received by solar PV panels on an hourly basis can be evaluated from the horizontal radiation data on direct radiation (I_{DH}, W/m^2) and scattered radiation (I_{SH}, W/m^2) in the GEOS-5 database (Lucchesi, 2017). The total radiation received by the panels (I_T) is the sum of those three streams of radiation:

$$R_{DT} = \frac{\cos\theta \times \sinh + \sin\theta \times \cosh \times \cos\alpha}{\sinh} \quad \text{(Equation 9)}$$

$$I_{DT} = I_{DH} \times R_{DT} \quad \text{(Equation 10)}$$

$$I_{ST} = I_{SH}[0.5 \times (1 + \cos\theta)] \quad \text{(Equation 11)}$$

$$I_{RT} = 0.5\rho(I_{DT} + I_{ST}) \times (1 - \cos\theta) \quad \text{(Equation 12)}$$

$$I_T = I_{DT} + I_{ST} + I_{RT} \quad \text{(Equation 13)}$$

where α and h are hourly solar azimuth and solar altitude, respectively; ρ is ground reflectivity, taken as 0.2 here (Chen et al., 2019); and I_T is the total radiation received by the panel.

Temperature influence

In practice, working efficiency of solar PV panels are influenced by the ambient temperature. An increase in PV panel surface temperature from the test operation conditions would reduce operation efficiency from its maximum value. The hourly efficiency adjusted by the influence of ambient temperature, F_{TEM}, can be calculated as follows:

$$T_{PVB} = T_{ENV} + \left(\frac{NOCT - 20}{0.8}\right) \times I \quad \text{(Equation 14)}$$

$$F_{TEM} = 1 + \sigma \times (T_{PVB} - 25^{\circ}C) \quad \text{(Equation 15)}$$

where T_{PVB} and T_{ENV} are the panel surface temperature and ambient temperature, respectively; NOCT is the normal operation cell temperature, which is 45 °C[75]; σ is the peak power coefficient (−0.35%/ °C), and F_{TEM} identifies the panel efficiency adjusted by temperature.

Hourly power outputs

In the present analysis, we selected typical polysilicon 375Wp modules (LONGi, 2021), which occupy a relatively large share of China's solar PV market, with a panel power efficiency, F_{con}, of 20.6%. System efficiency F_{sys}, with comprehensive consideration of nine factors of the whole process (from power production to grid connection), was determined at 80.96% (see Table S8). The final power outputs of the RSPV can be expressed as:

$$Power_{i,j}[W \cdot h] = Area_i \times RF_{ratio} \times I_{T(j)}\left[\frac{W \cdot h}{m^2}\right] \times F_{con} \times F_{TEM} \times (1 - F_{\mathrm{PVSHD}}) \times f_{shade} \times F_{con} \times F_{sys} \quad \text{(Equation 16)}$$

where $Power_{i,j}$ is the power generation in the jth hour of the ith building in the area, $Area_i$ is the suitable area of the ith building in the area, $I_{T(j)}$ is the radiation intensity on the surface of solar panels on the jth hour, F_{con} is the panel power efficiency, and the remaining parameters were defined above.

POWER SYSTEM PLANNING & OPTIMIZATION MODEL FOR THE RSPV + SYSTEM

The flexible operation of building-related loads including EVs, ACs as well as heat storage from TES were modeled to accommodate the intermittency and fluctuation of RSPV generation. "For Beijing's case, we excluded battery storage as flexibility options mainly for two reasons. On one hand, the RSPV electricity could only be stored in batteries for a short period usually within 24 h, making it difficult for batteries to play a major role in consuming RSPV electricity in the long-term across seasons. On the other hand, the application of battery storage has aroused security concerns in densely built mega-cities in China (Chuneng.BJX, 2021), and to place battery storage inside the buildings is against China's current fire control design requirements (ESCN, 2021). Two charging modes were considered for EVs: the quick-charging and slow-charging methods. We assumed 50% of quick-charging load is adjustable while all the slow-charging allows the loads to move from one period to another (Saxena et al., 2015). Here, we assumed that the storage for AC mainly included two types: daily and seasonal thermal energy storage (TES). The daily TES was considered to be daily balanced while the seasonal TES was considered to be yearly balanced. Apart from RSPV generation, the electricity from the power grid could also be used to supply the load.

In the PSP&O model, the output of RSPV generation and external power supply were separately constrained by the installation capacity of RSPV units and transmission line capacity. Actual charging behaviors of slow- and quick-charging EV loads in each period were limited by total predicted charging power capacity and the maximum percentage of adjustable loads. As for AC load, the actual flexible AC load was limited by the installed capacities of daily and seasonal TES.

The decision variables in the PSP&O model include hourly energy supply, consumption and energy storage state across three sectors: hourly power supply for different generation, load shifting for EVs and hourly energy supply and consumption from TES. $p^{E}_{d,t}$ and $p^{PV}_{d,t}$ represent respectively the generation of external power supply and scheduled output of PV generation at t hour in d day ($d \in [1,D], t \in [1,T]$). $I^{Q,EV,FW}_{d,t}$, $I^{Q,EV,BW}_{d,t}$ and $I^{S,EV,FW}_{d,t}$, $I^{S,EV,BW}_{d,t}$ respectively represent forward and backward shifting load of quick- and slow-charging EVs at t hour in d day, and $E^{EV}_{d,t}$ represents the shifted electricity for EVs at t hour in d day. $I^{DS,AC,Cha}_{d,t}$ and $I^{DS,AC,Dis}_{d,t}$ respectively represent charging and discharging of daily TES for AC load at t hour in d day, while $I^{SS,AC,Cha}_{d,t}$ and $I^{SS,AC,Dis}_{d,t}$ respectively represent charging and discharging of seasonal TES for AC load at t hour in d day. $E^{DS,AC}_{d,t}$ and $E^{SS,AC}_{d,t}$ represent the inventory of the daily and seasonal TES for ACs at t hour in d day, respectively. All the parameters and variables for the power PSP&O model are summarized as nomenclature in Table S17.

The model minimizes the total costs from both annualized investment cost C^{Inv} and year-round operation expense C^{Ope} (Equation 17). The total net present value of investment cost comprises of the investment in

the external transmission, the daily and seasonal storage (Equation 18). Equation 19 calculates the annualized investment cost based on the total net present value $C^{Inv,Pre}$ divided by the annuity present value coefficient of the entire investment life. represents the investment payback year and γ is the discount ratio. The operation cost only includes variable cost of external transmission power as well as operation and maintenance (O&M) cost of RSPV $C^{O\&M,RSPV}$ and thermal storage $C^{O\&M}$ (Equation 20). Equation 21 represents the O&M cost calculation of RSPV. $\overline{p}^{RSPV}$ represents the installed capacity of RSPV. The unit O&M cost of the RSPV $c^{O\&M,RSPV}$ is set as 75 CNY/kW/year (Walker, 2017), while the O&M cost of the thermal storage is assumed as 1% of the storage's capital investments (Yang et al., 2021).

$$\text{minimize } C^{Inv} + C^{Ope} \quad \text{(Equation 17)}$$

$$C^{Inv,Pre} = C^{E,Inv} \cdot p^{E} + \left(C^{DSP,Inv} \cdot \overline{p}^{DS,AC} + C^{DSE,Inv} \cdot \overline{E}^{DS,AC}\right) + \left(C^{SSP,Inv} \cdot \overline{p}^{SS,AC} + C^{SSE,Inv} \cdot \overline{E}^{SS,AC}\right) \quad \text{(Equation 18)}$$

$$C^{Inv} = C^{Inv,Pre} \cdot ((1+\gamma)^{P} - 1)/\gamma(1+\gamma)^{P} \quad \text{(Equation 19)}$$

$$C^{Ope} = \sum_{d=1}^{D} \sum_{t=1}^{T} C^{E,Ope} \cdot p_{t,t}^{E} + C^{O\&M,RSPV} + C^{O\&M,TES} \quad \text{(Equation 20)}$$

$$C^{O\&M,RSPV} = c^{O\&M,RSPV} \cdot \overline{p}^{RSPV} \quad \text{(Equation 21)}$$

where $C^{E,Inv}$ and p^{E} respectively represent the unit capital cost of external power transmission and required of additional external power supply. $\overline{p}^{DS,AC}$ and $\overline{p}^{SS,AC}$ represent respectively power capacity of daily and seasonal TES for ACs, while $C^{DSP,Inv}$ and $C^{SSP,Inv}$ represent respectively their unit costs. $\overline{E}^{DS,AC}$ and $\overline{E}^{SS,AC}$ represent respectively energy capacity of daily and seasonal TES for ACs while $C^{SSE,Inv}$ and $C^{DSE,Inv}$ represent respectively their unit costs. $p_{d,t}^{E}$ represents the generation of external power supply at t hour in d day, and $C^{E,Ope}$ represents the unit power price (see Table S15).

The model considers the constraints from power balance, load shifting of EVs, charging/discharging of TES and the regulated RSPV utilization ratio. Equation 22 is the generation-load balance equation, which ensures the aggregated output of external power supply and RSPV generation units to meet the load demand on an hourly basis. Given the adjustable shifting characteristics of EV and AC load, the electricity load demand could be advanced or delayed in the time domain. The loads of quick-charging EVs and show-charging EVs would change to $I_{d,t}^{Q,EV} + (I_{d,t}^{Q,EV,FW} - I_{d,t}^{Q,EV,BW})$ and $I_{d,t}^{S,EV} + (I_{d,t}^{S,EV,FW} - I_{d,t}^{S,EV,BW})$ at t hour in d day, respectively. Two kinds of thermal storage are considered to supply the AC load, namely the daily and seasonal TES. Therefore, the charging power $I_{d,t}^{DS,AC,Cha}$, $I_{d,t}^{SS,AC,Cha}$ and discharging power $I_{d,t}^{DS,AC,Dis}$, $I_{d,t}^{SS,AC,Dis}$ could also adjust the load of ACs with storage. Meanwhile, Equation 23 ensures that the output of external power supply does not exceed the upper and lower limits from the power system transmission constraints. Equation 24 indicates that the RSPV generation units should be scheduled less than or equal to their available power output.

$$\text{s.t.} \quad p_{d,t}^{E} + p_{d,t}^{PV} = I_{d,t}^{Q,EV} + \left(I_{d,t}^{Q,EV,FW} - I_{d,t}^{Q,EV,BW}\right) + I_{d,t}^{S,EV} + \left(I_{d,t}^{S,EV,FW} - I_{d,t}^{S,EV,BW}\right) + I_{d,t}^{AC} + \left(I_{d,t}^{DS,AC,Cha} - I_{d,t}^{DS,AC,Dis}\right) + \left(I_{d,t}^{SS,AC,Cha} - I_{d,t}^{SS,AC,Dis}\right), \quad \forall d,t \quad \text{(Equation 22)}$$

$$\underline{p}^{E} \le p_{d,t}^{E} \le \overline{p}^{E}, \forall d,t \quad \text{(Equation 23)}$$

$$0 \le p_{d,t}^{PV} \le w_{d,t}, \forall d,t \quad \text{(Equation 24)}$$

where $I_{d,t}^{Q,EV}$ and $I_{d,t}^{S,EV}$ represent the load of quick- and slow-charging of EVs, $I_{d,t}^{AC}$ represents the AC cooling and heating load, $\overline{p}^{E}$ and $\underline{p}^{E}$ respectively represent upper and lower limits of the external power supply, and $\omega_{d,t}$ represents available power output of RSPV generation in at t hour in d day.

For the constraints of EVs, Equation 25 and Equation 26 limit the actual load demand of slow- and quick-charging EVs at t hour in d day. Equation 27 calculates the shifted EV load at t hour in d day. Equation 28 sets the upper limit for the shifted EV load, with the assumption that 100% of the slow-charging and 50% of quick-charging load are adjustable. Equation 29 balances the shifted EV load in one day so that the shifted electricity load still fully satisfies the total electricity demand from EVs within the day.

$$0 \le I_{d,t}^{S,EV} + \left(I_{d,t}^{S,EV,FW} - I_{d,t}^{S,EV,BW}\right) \le \overline{I}^{S,EV} \quad \text{(Equation 25)}$$

$$0 \le I_{d,t}^{Q,EV} + \left(I_{d,t}^{Q,EV,FW} - I_{d,t}^{Q,EV,BW}\right) \le \overline{I}^{Q,EV} \quad \text{(Equation 26)}$$

$$E_{d,t}^{EV} = E_{d,t-1}^{EV} + \left(I_{d,t}^{EV,BW} - I_{d,t}^{EV,FW}\right), \forall d, t \ge 2 \quad \text{(Equation 27)}$$

$$E_{d,t}^{EV} \le \overline{E}_{d,t}^{EV} \quad \text{(Equation 28)}$$

$$E_{d,1}^{EV} = E_{d,T}^{EV} \quad \text{(Equation 29)}$$

where $\overline{I}^{Q,EV}$ and $\overline{I}^{S,EV}$ represent respectively power capacities of the quick- and slow-charging devices for EVs, and $\overline{E}^{EV}$ represents the maximum EV load that could be shifted.

For the constraints of ACs, Equation 30 and Equation 31 indicate the charging and discharging power should not exceed the total power capacities of the daily and seasonal TES. Equation 32 formulates the operation equation in the neighboring hours. As expressed in Equation 33, the first equation describes the seasonal TES inventory change between neighboring hours in the same day, and the second one links the end hour of the first day and the start hour of the following day. Equation 34 sets the upper limits for the inventory of the daily and seasonal TES. Equation 35 balances the inventory of the daily and seasonal TES. The daily and seasonal TES inventories are considered to be daily balanced and annually balanced, respectively.

$$I_{d,t}^{DS,AC,Cha}, I_{d,t}^{DS,AC,Dis} \le \overline{P}^{DS,AC} \quad \text{(Equation 30)}$$

$$I_{d,t}^{SS,AC,Cha}, I_{d,t}^{SS,AC,Dis} \le \overline{P}^{SS,AC} \quad \text{(Equation 31)}$$

$$E_{d,t}^{DS,AC} = E_{d,t-1}^{DS,AC} + \left(I_{d,t}^{DS,AC,Cha} - I_{d,t}^{DS,AC,Dis}\right), \forall d, t \ge 2 \quad \text{(Equation 32)}$$

$$\begin{cases} E_{d,t}^{SS,AC} = E_{d,t-1}^{SS,AC} + \left(p_{d,t}^{SS,AC,Cha} - p_{d,t}^{SS,AC,Dis}\right), \forall d, t \ge 2 \\ E_{d,1}^{SS,AC} = E_{d-1,T}^{SS,AC} + \left(p_{d,1}^{SS,AC,Cha} - p_{d,1}^{SS,AC,Dis}\right), \forall d \ge 2 \end{cases} \quad \text{(Equation 33)}$$

$$E_{d,t}^{DS,AC} \le \overline{E}^{DS,AC}, E_{d,t}^{SS,AC} \le \overline{E}^{SS,AC} \quad \text{(Equation 34)}$$

$$E_{d,1}^{DS,AC} = E_{d,T}^{DS,AC}, E_{d,1}^{SS,AC} = E_{D,T}^{SS,AC} \quad \text{(Equation 35)}$$

Equation 36 defines the constraint of the PV electricity utilization ratio α, which is defined as 100% in this study.

$$\sum_{d}^{|\mathbb{D}|} \sum_{t}^{|\mathbb{T}|} p_{d,t}^{PV} = \alpha \sum_{d}^{|\mathbb{D}|} \sum_{t}^{|\mathbb{T}|} w_{d,t}, \forall d, t \quad \text{(Equation 36)}$$

As a Linear Programming model, the model is solved using CPLEX 12.5.